Calculation of the electromagnetic moments and electroexcitation form factors for some boron isotopes using shell model with skyrme interaction

A. A. Alzubadi and G. W. Harby

Department of Physics, College of Science, University of Baghdad, Baghdad, Iraq.
e-mail: ali.kareem@sc.uobaghdad.edu.iq

Received 2 April 2022; accepted 8 May 2022

The magnetic dipole and electric quadrupole moments for some Boron isotopes were calculated using the shell model taking into account the effect of the two-body effective interactions and the single-particle potentials. These isotopes are; $(^{8}_{5})$B(2^{+}), $(^{1}_{5}0)$B(3^{+}), $(^{1}_{5}1)$B$((3/2)^{-})$, $(^{1}_{5}2)$B(1^{+}) and $(^{1}_{5}3)$B$((3/2)^{-})$. Also, the elastic and inelastic longitudinal and transverse electron scattering form factors are calculated for ^{10}B and ^{11}B, for which there are available experimental data. The one-body transition density matrix elements (OBDM) were calculated using the two-body effective interactions; PWT, PEWT, PKUO and CKIHE, which are carried out in the p-shell model space. Skyrme interaction was implemented to generate the single-particle matrix elements with Hartree-Fock approximation and compared with those of harmonic-oscillator and Wood-Saxon potentials. All the evaluated results were compared with available experimental data. The present work has led us to conclude that the shell model calculations with Skyrme type interaction give a good tool for nuclear structure studies. All signs for the experimental electromagnetic moments data are reproduced correctly. The longitudinal and transverse form factors for positive and negative parity states are fairly well reproduced when using a suitable model space.

Keywords: Nuclear magnetic dipole; electric quadrupole; electroexcitation form factor; skyrme interaction.

DOI: https://doi.org/10.31349/RevMexFis.69.011202

1. Introduction

Calculations of the magnetic dipole and electric quadrupole moments are considered one of the most important ways to learn about the nuclear structure, and to obtain very dense and deep information in this field like deformations, charge, and nuclear moments. Electromagnetic moments are considered to be amongst the most basic probes, one can use to obtain information about the nuclear structure throughout the entire nuclear chart. The magnetic moments of nuclei are highly sensitive to the orbits occupied by the valence nucleons, where magnetic moments offer a perfect test of the purity of a specific configuration mixing shell model [1]. As for the deformation, the electric quadrupole moment is considered a measure of nuclear deformation. The differences in their magnitudes and signs vary as a function of the charge number, A, and mass, and atomic number, Z, are sensitive measures of the many-particle structures of the nuclear wave functions. The shape of nuclei and magnitudes of deformation is given by the quadrupole moments, are can be classified as an oblate ($Q2 < 0$) or prolate ($Q2 > 0$) [2]. It is well known that the nuclei with an odd number of protons and or neutrons have an intrinsic spin they also in general possess a magnetic dipole moment. The nuclear magneton μ_N is a unit of experimental magnetic moments but experimental methods tend to act as measures of the nuclear g factor. However, in both cases, this represents a way to calculate the unknown spin of an exotic nuclear state. This can be achieved by comparing the experimental magnetic moment to model calculations or by comparing the values of a similar state to the measured values, so the shell structure of single-particle levels in a spherical potential can be affected by the nuclear deformation [3].

In the present work, the electromagnetic moments for some Boron isotopes will be calculated using the shell model, taking into account the effect of the two-body effective interactions and the single-particle potentials. Also, the longitudinal and transverse electron scattering form factors for isotopes for which there are available experimental data. The p-shell model space will be used for this purpose, which consists of the active shells $1p_{1/2}$, $1p_{3/2}$, above the inert ^{4}He nucleus core $(1s)^4$, which remains closed.

2. Theoretical consideration

The nuclear matrix element of the electromagnetic (O) and electron scattering (T) operators is expressed as the sum of the products of the one-body transition density matrix ($OBDM$) times the single-particle matrix elements [4]

$$\langle f\|\hat{X}(\lambda)_{t_z}\|i\rangle = \sum_{k_a k_b} OBDM(fik_ak_b\lambda) \times \langle k_a\|\hat{X}(\lambda)_{t_z}\|k_b\rangle, \quad (1)$$

where X operator stands for O or T operators for electromagnetic and electron scattering operators, respectively. The $OBDM$ is given by

$$OBDM(fik_ak_b\lambda) = \frac{\langle\|[a^{+}_{k_a}\otimes\tilde{a}_{k_b}]^{\lambda}\|i\rangle}{\sqrt{2\lambda+1}}, \quad (2)$$

where i and f include all the quantum numbers needed to distinguish the states. The nuclear magnetic dipole moment is defined in terms of the $M1$ operator as [5]

$$\mu = \sqrt{\frac{4\pi}{3}} \begin{pmatrix} J & 1 & J \\ -J & 0 & J \end{pmatrix} \sum_{t_z} \langle J \| \hat{O}(M1)_{t_z} \| J \rangle \mu_N, \quad (3)$$

where μ_N is the nuclear magneton $\mu_N = e\hbar/2m_pc = 0.1051$ efm. The electric quadrupole moment is defined in terms of the $E2$ operator as

$$Q = \sqrt{\frac{16\pi}{5}} \begin{pmatrix} J & 1 & J \\ -J & 0 & J \end{pmatrix} \sum_{t_z} \langle J \| \hat{O}(E2)_{t_z} \| J \rangle e_{t_z}, \quad (4)$$

where the initial and final nuclear states $|J\rangle$ include all the quantum numbers needed to distinguish the nuclear states.

For the central potential, the Skyrme potential is used; it is a two-body interaction. One may generate from it a one-body potential in the Hartree-Fock (HF) approximation. It is a mean-field potential and it is supposed to provide the mean-field due to all the nucleons which compose the nucleus and approximates the realistic nucleon-nucleon (and nucleon-nucleon-nucleon) forces. The Skyrme potential VSkyrme can be written as [6]

$$\begin{aligned} V_{\text{skyme}}(\vec{r}_1\vec{r}_2) &= t_0(1 + x_0\hat{P}_\sigma)\delta_{12} + \frac{t_1}{2}(1 + x_1\hat{P}_\sigma)[\vec{k}'^2\delta_{12} + \delta_{12}\vec{k}^2] + t_2(1 + x_2\hat{P}_\sigma)\vec{k}'\delta_{12}\vec{k} \\ &+ \frac{t_3}{6}(1 + x_3\hat{P}_\sigma)\rho\left(\frac{\vec{r}_1 + \vec{r}_2}{2}\right)^\alpha \delta_{12} + iW_0\vec{k}'\delta_{12}(\vec{\tilde{\sigma}}_1 + \vec{\tilde{\sigma}}_2) \times \vec{k} + \frac{t_e}{2}\left(\left[3(\vec{\tilde{\sigma}}_1 \cdot \vec{k}')(\vec{\tilde{\sigma}}_2 \cdot \vec{k}') - (\vec{\tilde{\sigma}}_1 \cdot \vec{\tilde{\sigma}}_2)\vec{k}'^2\right]\delta_{12}\right. \\ &\left. + \delta_{12}\left[3(\vec{\tilde{\sigma}}_1 \cdot \vec{k})(\vec{\tilde{\sigma}}_2 \cdot \vec{k}) - (\vec{\tilde{\sigma}}_1 \cdot \vec{\tilde{\sigma}}_2)\vec{k}^2\right]\right) + t_0\left[3(\vec{\tilde{\sigma}}_1 \cdot \vec{k})\delta_{12}(\vec{\tilde{\sigma}}_2 \cdot \vec{k}) - (\vec{\tilde{\sigma}}_1 \cdot \vec{\tilde{\sigma}}_2)\vec{k}'\delta_{12}\vec{k}\right], \end{aligned} \quad (5)$$

where $\delta_{12} = \delta(\vec{r}_1 - \vec{r}_2)$ and k, k' are the relative momentum operators with k acting on the right, while k' is the operator acting on the left and given by

$$\hat{k} = \frac{1}{2i}(\vec{\nabla}_1 - \vec{\nabla}_2), \quad \hat{k}' = \frac{1}{2i}(\vec{\nabla}_1 - \vec{\nabla}_2), \quad (6)$$

and $\hat{P}_\sigma$ is the spin-exchange operator that is given as

$$\hat{P}_\sigma = \frac{1}{2}(1 + \vec{\sigma}_1 \cdot \vec{\sigma}_2). \quad (7)$$

The electroexcitation form factors for elastic and inelastic scattering are denoted by the longitudinal Coulomb form factor, $F(C\lambda, q, f, i)$, the transverse electric $F(E\lambda, q, f, i)$, and the transverse magnetic $F(M\lambda, q, f, i)$, form factors, where λ is the multipolarity [7]. The last two types of form factors can be divided into the components according to the convection currents λ_c (due to the orbital motion of the nucleons) and the magnetization currents λ_m (due to the intrinsic magnetic moments of the nucleons), respectively. Therefore, the total longitudinal form factor can be written as

$$|F_C(q, f, i)|^2 = \sum_{\lambda \geq 0} |F(C\lambda, q, i, f)|^2, \quad (8)$$

and the total transverse form factor as

$$\begin{aligned} |F_T(q, f, i)|^2 = \sum_{\lambda > 0} \big\{ &|F(E\lambda, q, i, f)|^2 \\ &+ |F(M\lambda, q, i, f)|^2 \big\}. \end{aligned} \quad (9)$$

Electroexcitation form factor involving angular momentum λ and momentum transfer q, between the initial (i) and final (f) nuclear shell model states can be written as [8]

$$\begin{aligned} |F(\eta\lambda, q)|^2 = &\frac{4\pi}{Z^2(2J_i + 1)} \\ &\times |\langle f \| \hat{T}(\eta\lambda, q) \| i \rangle F_{\text{c.m}}(q) F_{\text{f.s}}(q)|^2, \end{aligned} \quad (10)$$

where η is the longitudinal or Coulomb C, and transverse form factors, respectively. The finite size (f.s.) nucleon form factor superscript is the correction for the lack of translational invariance in the shell model. A is the mass number, and b is the harmonic oscillator (HO) size parameter.

3. Results and discussion

In the present research, we have adopted the p-shell model space in calculating the OBDM elements for low-lying positive parity states. Whereas for negative parity states the $spsdpf$ no core-shell model space with (0+1) $\hbar\omega$ restriction has been used. All the calculations were carried out using the NuShellX@MSU code [9]. It uses a J-coupled proton-neutron basis, and J-scheme matrix dimensions of up to the order of 100 million can be considered. The OBDM elements are then used to calculate the matrix elements of $C\lambda$, $E\lambda$, and $M\lambda$ operators. As we mentioned previously, the radial wave functions of the single-particle matrix elements were calculated using a two-body Skyrme interaction potential with SLy4 parametrization in addition to the HO and Wood-Saxon (WS). Discussion of the results will be divided into three sections, the first one is devoted to the magnetic dipole moment, the second section examines the electric quadrupole moments followed by the electroexcitation form factors which are reported in the third section.

3.1. Magnetic dipole moments

The magnetic dipole moments (μ) are calculated for Boron isotopes in p-shell model space using four two-body effective interactions; PWT, PEWT, PKUO and CKIHE with free

TABLE I. Theoretical calculated of magnetic dipole moment μ(nm) for B-isotopes using four interactions (PWT, PEWT, PKUO and CKIHE) in comparison with experimental data taken from Ref. [10].

Isotopes	J^π	PWT	PKUO	CKIHE	PEWT	Exp [10]
8	2^+	1.201	1.155	0.76	1.489	1.03579(5)
10	3^+	1.809	1.85	1.804	1.838	1.80064 (6)
11	$3/2^-$	2.445	2.414	2.013	2.759	2.68864 (10)
12	1^+	0.804	-0.04	0.48	0.885	1.00272(11)
13	$3/2^-$	3.026	2.972	3.011	3.252	3.1778 (5)

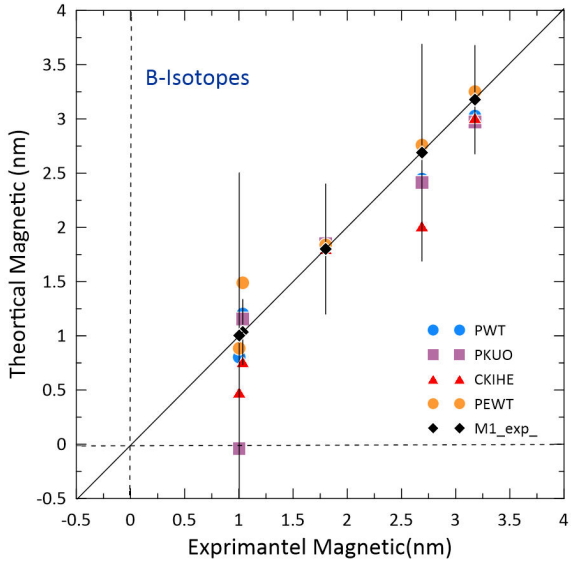

FIGURE 1. The calculated magnetic dipole moments μ(nm)vs the experimental data for B-isotopes using different two-body effective interactions; PWT, PEWT, PKUO and CKIHE.

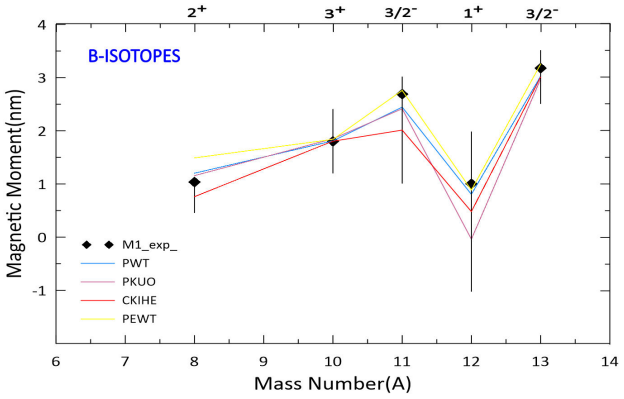

FIGURE 2. The calculated magnetic dipole moments μ(nm) for B-isotopes using different two-body effective interactions in comparison with the experimental data of Ref [10].

nucleon g factors. These interactions are reasonable for the p-shell model space calculations. The calculated results are presented in Table I in comparison with the experimental data taken from Ref. [10]. It has been found that the calculated results are concurring with experimental data. For more illustration, the comparison between the calculated μ moments with the corresponding experimental values is depicted in Figs. 1 and 2. It is obvious that the PEWT interaction gives results that are broadly consistent with experimental data. It is one of the recent versions of the p-shell model space effective interactions, which take into account a complete set of 77 p-shell energies in the mass region $A = 5-16$. Apart from this slight discordance, it can be noticed that all interactions concur for the 10 B isotope. This isotope lying in the middle of the lp shell has been a favourite testing ground for calculations of nuclear structure in the lp shell. One hallmark of this isotope is the existence of two low-lying l+ sates, the first and third excited states at 0.7183 and 2.1542 MeV. The properties of these states are sensitive to mixing between them, and the amount of mixing has been modified to enhance the agreement with experiment data.

3.2. Electric quadrupole moments

The electric quadrupole moments for the selected Boron isotopes are also calculated and presented in Table II in compa-

TABLE II. The theoretical calculated electric quadrupole moments in e^2fm^2 for B-isotopes using four interactions (PWT, PEWT, PKUO and CKIHE) in comparison with experimental data taken from Ref. [10].

Isotopes	J^π	PWT	PKUO	CKIHE	PEWT	Exp
8	2^+	4.59	5.73	3.66	5.11	6.43
10	3^+	9.41	8.88	9.48	8.96	8.45
11	$3/2^-$	5.28	4.96	5.39	4.88	4.05
12	1^+	2.08	0.75	1.55	1.63	1.32
13	$3/2^-$	4.94	4.99	4.98	4.59	3.65

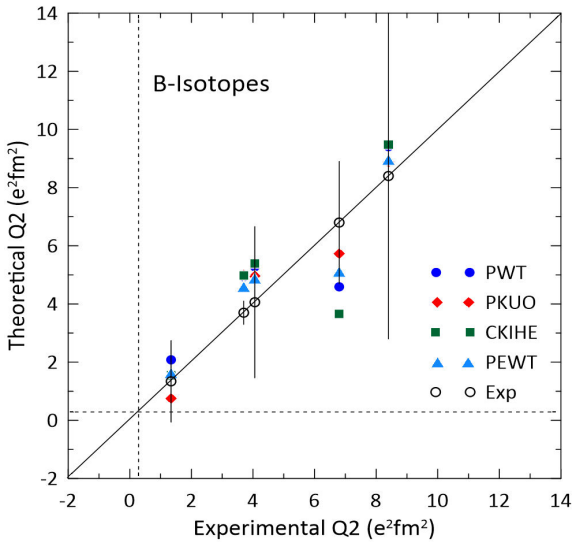

FIGURE 3. The calculated electric quadrupole moments $Q2$ e^{2}fm^2 vs the experimental data for B-isotopes using different two-body effective interactions; PWT, PEWT, PKUO and CKIHE.

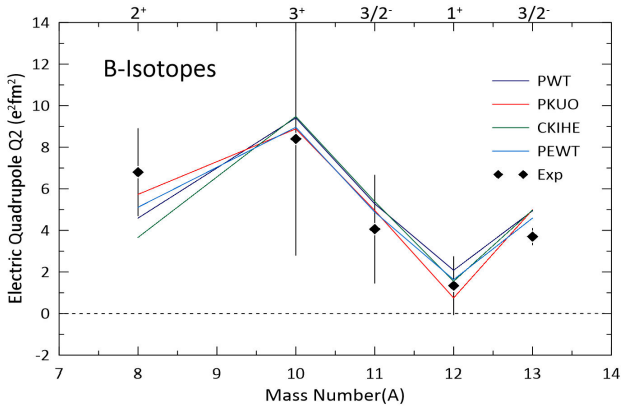

FIGURE 4. The calculated electric quadrupole moments $Q2$ e^{2}fm^2 for B-isotopes using different two-body effective interactions in comparison with the experimental data of Ref. [10].

parison with the available experimental data taken from Ref. [10]. From these results, it is clear that the calculations with p wave functions reasonably explain the experimental data and predict the correct sign (prolate deformation) for the quadrupole moments, as given in Table II and shown in Figs. 3 and 4. Furthermore, it has been found that there is no systematic trend guiding the calculated results in comparison with the experimental data. The highest Q value gets for B isotopes when ($A = 10$) and more precisely by using (CKIHE) interaction, while the less value gets at ($A = 12$) isotope by (PKUO) interaction. In general point of view, the data obtained using PKUO interaction gives the closest results to the experimental data. The matrix elements of this interaction are evaluated using the separation method for the singlet-even and triplet-even states and the reference spectrum method for the singlet-odd and triplet-odd states. The second-order Born term for the triplet-even tensor force is found to be very important in reproducing the experimental data.

After calculating the OBDMs for each isotope, we should adopt one-body potentials to be able to calculate the single-particle matrix elements. Unifying the interactions employed in HF computations would be a significant step forward. The zero-range density-dependent Skyrme-type interaction is one of the most successful and often utilized phenomenological interactions for HF calculations. Skyrme interaction is adopted to generate a one-body potential in HF theory to calculate the single-particle matrix elements in addition to the realistic WS and HO. Even better results are achieved, the applicability of the present method is tested in calculating the quadrupole moments using different single-particle potentials. Namely, the HO, WS [11], and, Skyrme Hartree-Fock (SHF) with SLy4 parameterization. From Table III and Figs. 5 and 6. It is clear that the calculated results using these types of potentials are in good correspond to the experimental data of quadrupole moments, except for the ^{8}B isotope. The ^{8}B isotope has a very small proton-separation energy of 136.4 keV [12], so it is speculated that the outer valence proton forms a halo structure, despite the existence of Coulomb and centrifugal barriers [13]. Moreover, our results using the shell model calculation with various single-particle potentials demonstrated that the enhancement of the Q moment cannot be connected mainly to the extra enhancement of a proton halo, because the last proton contributes destructively to the Q moment in the case of the ^{8}B isotope. Therefore, the Q moment has to be reproduced based on realistic deformation and realistic radial distribution, especially for the loosely bound nuclei [13].

TABLE III. The theoretical calculated electric quadrupole moments in e^2fm^2 for B-isotopes using three different single-particle potentials (HO, WS, and SLy4) in comparison with experimental data taken from Ref. [10].

Isotopes	J^π	HO	SLy4	WS	Exp
8	2^+	4.067	4.594	4.594	6.43
10	3^+	8.468	8.209	8.209	8.45
11	$3/2^-$	4.685	4.448	4.448	4.05
12	1^+	1.814	1.724	1.724	1.32
13	$3/2^-$	4.281	3.996	3.996	3.65

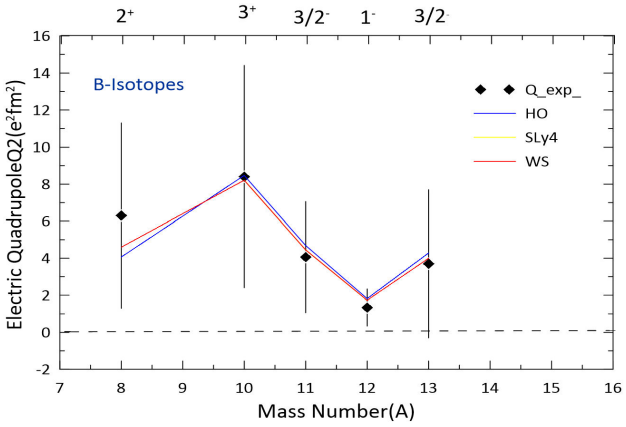

FIGURE 5. The calculated electric quadrupole moments $Q2$ e^{2}fm^2 for B-isotopes using different single-particle potentials in comparison with the experimental data of Ref [10].

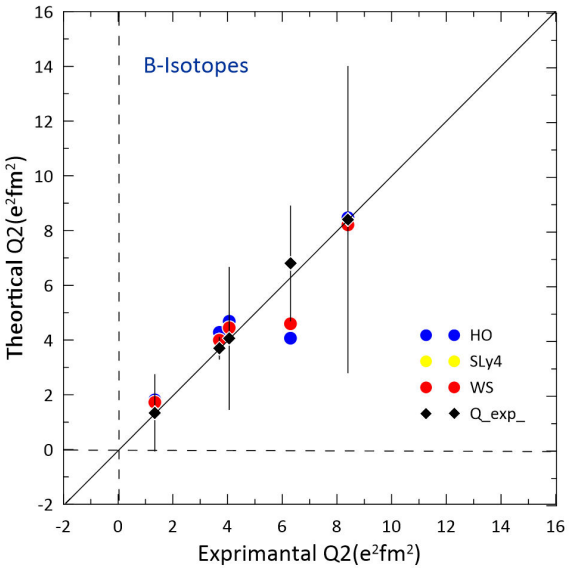

FIGURE 6. The calculated electric quadrupole moments $Q2$ e^{2}fm^2 vs the experimental data for B-isotopes using different single-particle potentials PWT, PEWT, PKUO and CKIHE.

3.3. Electroexcitation form factors

The elastic and inelastic longitudinal and transverse electron scattering form factors are calculated for ^{10}B and ^{11}B, for which there are available experimental data. The elastic longitudinal electroexcitation Coulomb form factors for the ground state of 10 B isotope 3^+, 0.0 MeV calculated with the p-shell model space wave functions using SLy4 parameterization (the same mean-field parametrization was used for calculating the moments), HO and WS are depicted in Fig. 7a) in comparison with experimental data taken from Ref. [14]. The allowed longitudinal multipoles C0 and C2 are also presented. It is obvious that the present results concur well with the general trend of the experimental data using WS potential in all momentum transfer region. Also, the elastic transverse magnetic electroexcitation form factors are presented in Fig. 7b). The allowed transverse multipoles for this state are Ml and M3. It can be noticed that the total form factor profiles are enhanced by the contribution of the M1 multipole. Although our calculated results differ slightly with experimental data of Ref. [14]. They bear a close resemblance with experimental data, especially in low momentum transfer

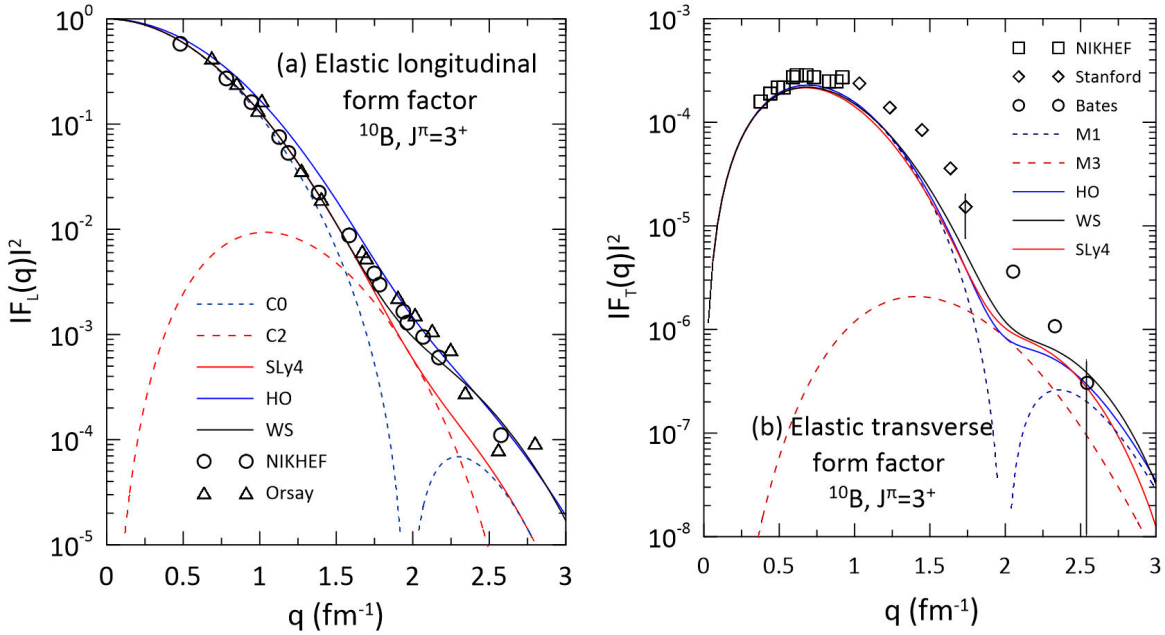

FIGURE 7. Theoretical longitudinal a) and transverse b) form factors for 3+, 0.0 MeV using SLy4 parameterization, HO and WS compared with experimental data taken from Ref. [14].

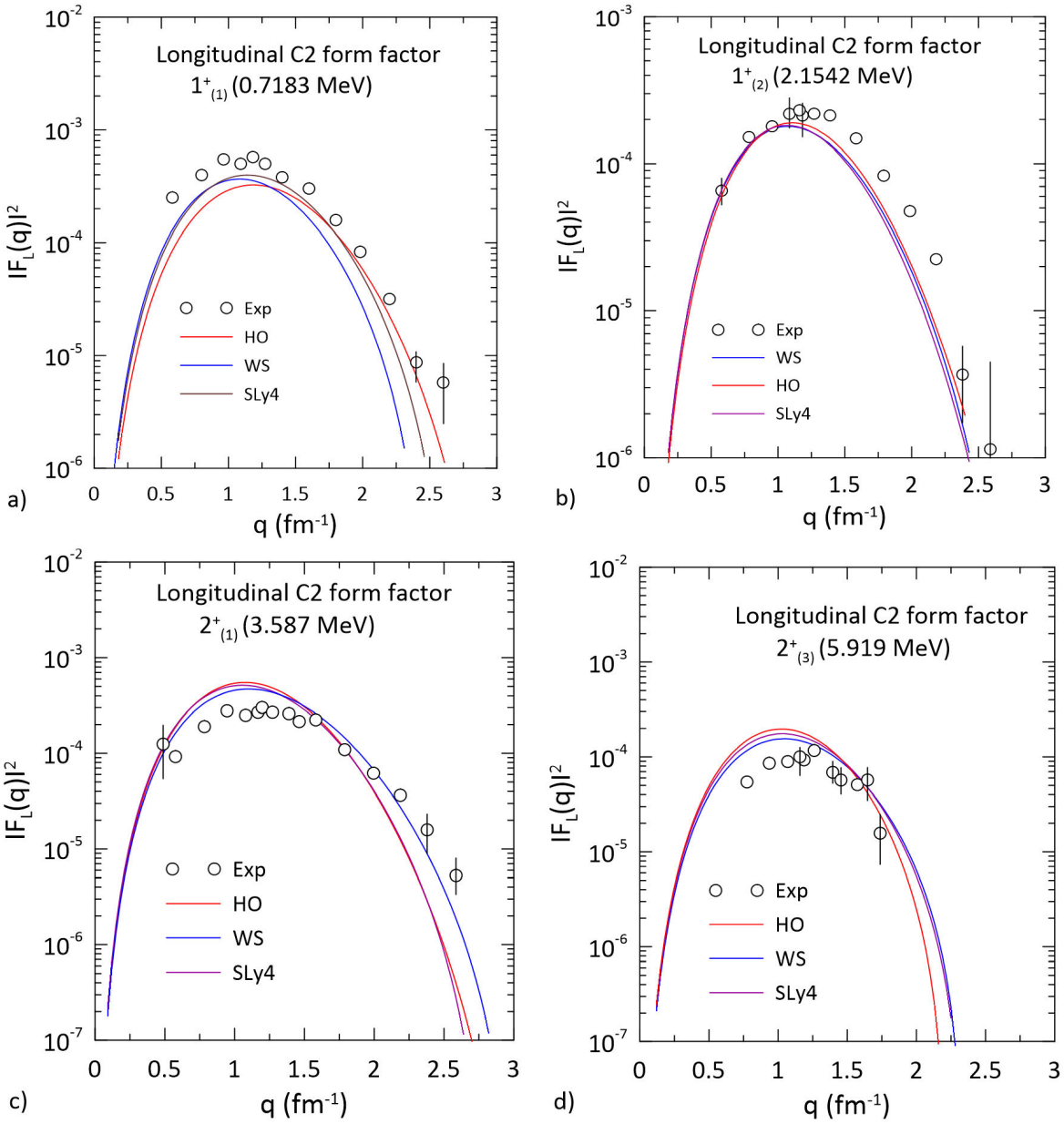

FIGURE 8. Theoretical longitudinal C2 form factors for a) 1^+ (0.7183 MeV), b) 1^+ (2.1542 MeV), c) 2^+ (3.587 MeV) and d) 2^+ (5.919 MeV) transitions using HO, WS and SLy4 parameterization compared with experimental data taken from Ref. [14].

region. Figure 8 shows the calculated inelastic longitudinal C2 electroexcitation form factors of transitions to even-parity isoscalar $T = 0$ states at 1^+ (0.7183 MeV), 1^+ (2.1542 MeV), 2^+ (3.587 MeV), and 2^+ (5.919 MeV). The longitudinal form factors all are dominated by the electric quadrupole transition C2 components. Although the C2 multipole is dominating, the curves in each case represent the sum of all conceivable multipole contributions. It is clear to observe that the 0.718 and 2.1542 MeV transitions are in reasonable agreement with experimental data in light of the fact that no parameters were changed to fit the experimental electron scattering data. Regarding the 2^+ (3.587 MeV), and 2^+ (5.919 MeV) transitions, it is obvious that the shape of the experimental form factor is thoroughly described by p-shell model space using the four potentials, although there is a slight deviation exists where the p-shell prediction underestimates the experimental data in low momentum transfer region. While in the high momentum transfer region, the WS potential provides a satisfying agreement with experimental data.

The p-shell predictions for transverse electroexcitation form factors for the same selected even-parity states are depicted in Fig. 9. The multipolarities included in these transitions are M1, E2, M3 multipoles. All of them have a significant contribution to the transverse form factors. From these figures it is clear that the theoretical calculations agree quite well with the general trends of the experimental electron scattering data.

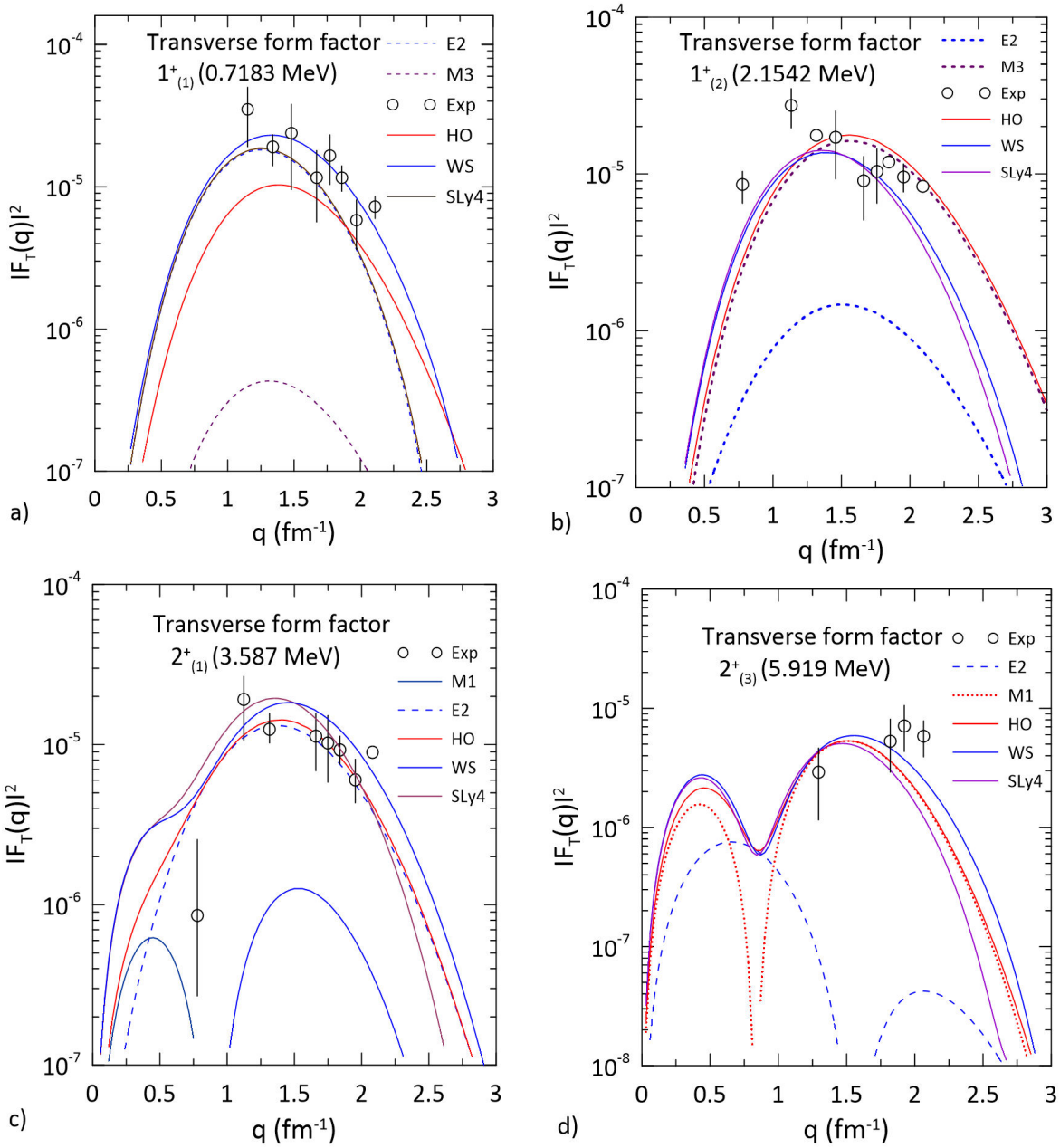

FIGURE 9. Theoretical transverse form factors for a) 1^+ (0.7183 MeV), b) 1^+ (2.1542 MeV), c) 2^+ (3.587 MeV) and d) 2^+ (5.919 MeV) transitions using HO, WS and SLy4 parameterization compared with experimental data taken from Ref. [14].

In general point of view, there is no systematic variation observed in the transverse form factors when changing the single-particle potentials. Even though the SLy4 and HO potentials succeed to reproduce the major trend of the experimental data of the transition 2^+ (3.587 MeV). The HO size parameter ($b = 1.75$ fm) was expected to be the same as that obtained via a fit to the p-shell nuclei charge radii. A slightly lower value would almost probably increase the experiment's agreement.

Inelastic transverse and longitudinal Coulomb electroexcitation form factors for the transition to the 2^+ (5.164 MeV) isovector T=1 state are shown in Figs. 10a) and b). In this transition, the contributing multipoles are the transverse M1, E2, M3 and longitudinal C2 multipoles. Inspection of these patterns indicates that the transverse form factor is mainly dominated by the influence of the M3 multipole, while the longitudinal is dominated by C2 multipole. A comparison was performed with the experimental data given in Ref. [14]. Because of the M3 component's dominance, it is acceptable to utilize the HO size parameter ($b = 1.5$ fm) to fit the form factor, which gives overall agreement with experimental data over the entire range of momentum transfer. As also depicted in Fig. 10, the C2 form factor is in reasonable agreement with the experimental data. Despite the lack of precision of the experimental data, they are nevertheless comparable.

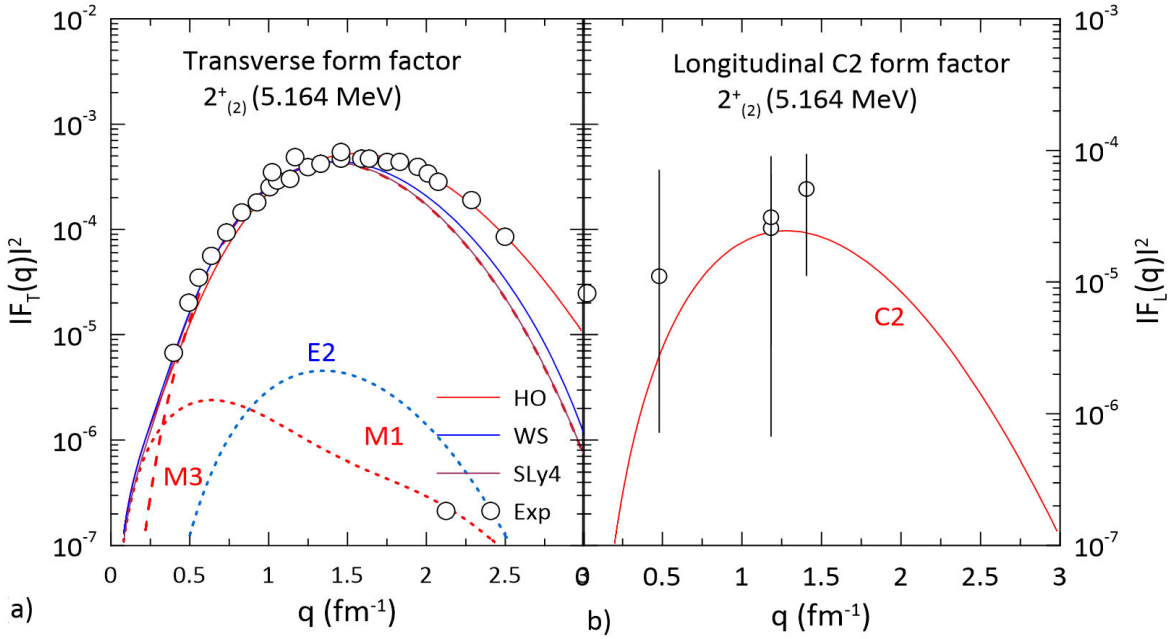

FIGURE 10. Theoretical transverse form factors a) and longitudinal b) for the transition to the 2^+ (5.164 MeV) state using HO, WS and SLy4 parameterization in comparison with experimental data taken from Ref. [14].

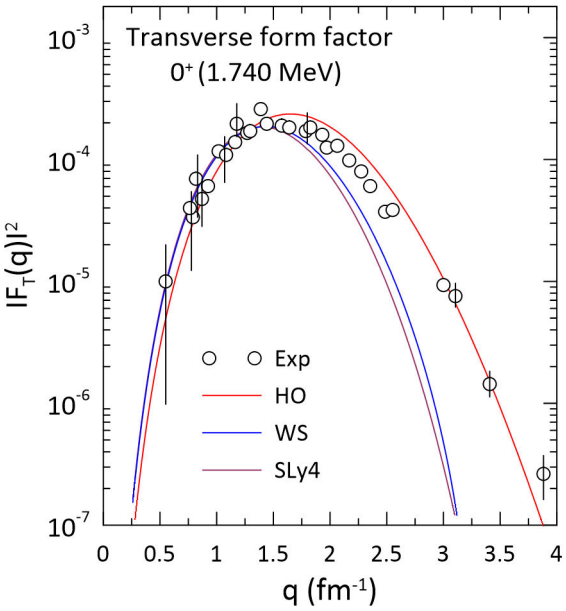

FIGURE 11. Theoretical transverse form factors for the transition to the 0^+ (1.740 MeV) state using HO, WS and SLy4 parameterization in comparison with experimental data taken from Ref [14].

Figure 11 shows the calculated transverse magnetic electroexcitation form factor for the transition from the ground state to the 0^+ (1.740 MeV) $T = 1$ state using SLy4 parameterization, together with the experimental data. It's worth mentioning in this context, it is a pure M3 transition. We can notice that the p-shell predication reproduces the experimental data more accurately with HO than SLy4 and WS, where the calculated form factor profile lies in fine quantitative agreement with experimental data.

Regarding the transition to the negative parity (unnatural-parity) states, larger spaces are needed to fully converge the excitation energies for the transition to these such states. The correct description of the inelastic form factor for negative parity states needs a vast number of basis states to reproduce the correct form. Therefore, the $spsdpf$ no-core shell model space (NCSM) with (0+1) $\hbar\omega$ truncation has been used to evaluate the OBDM elements. It is different from past shell-model calculations since we can allow all A nucleons to be active in the model space [11]. It includes four shells, $1s$, $1p$, $2s-1d$, and $1f-2p$. It turns out that many of the basis states used in the NCSM calculations are irrelevant to the description of any particular eigenstate. Therefore, after identifying the important basis states beforehand, one could reduce the dimension of the matrix eigenvalue problem without losing predictive power. The two-body effective interactions involved in this model space were founded by Warburton and Brown [15]. The single-particle matrix elements were calculated using SHF potential with SLy4 parameterization. Figure 12 depicts the total longitudinal and transverse form factors evaluated from the transitions to the odd parity $T = 0$ states 2- (5.1103 MeV) and 3- (6.129 MeV). According to these forecasts, it is obvious that $spsdpf$ predictions with SLy4 potential are in reasonable agreement with the general trend of the experimental data, although in the 2- state, they slightly underestimate these data at low momentum transfer region.

In this context, it is clear that the total longitudinal form factor is dominated by the C3 multipole in 2^- state, whereas the C1 multipole contribution is significant in the 3^- state.

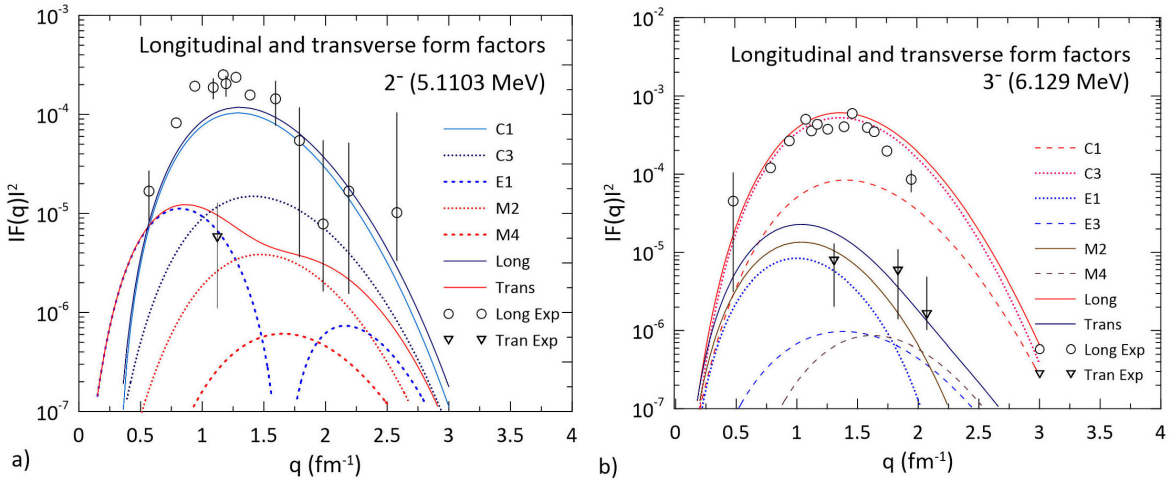

FIGURE 12. Theoretical longitudinal and transverse form factors for the transition to the 2^- (5.1103 MeV) state a) and for the 3^- (6.129 MeV) state b), using SLy4 parameterization in comparison with experimental data taken from Ref. [14].

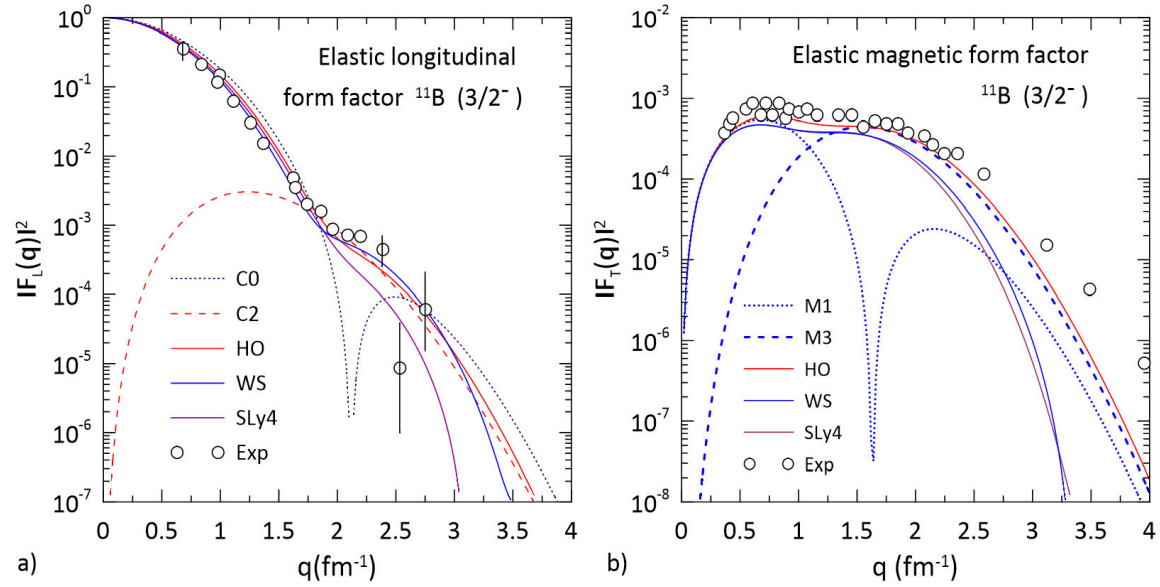

FIGURE 13. Theoretical total longitudinal a) and transverse b) form factors for the ground state of ^{11}B $3/2^-$ isotope, using HO, WS and SLy4 parameterization in comparison with experimental data taken from Refs. [16,17].

Of particular note, we can get spectacular results of the electroexcitation form factors for positive and negative parity states when choosing the suitable truncation for the NCSM.

^{11}B, $J^\pi = 3/2^-$, is the second isotope for which the experimental form factor data are available. Therefore, the elastic longitudinal and transverse electroexcitation form factors and their contribution were calculated using the selected potentials and shown in Fig. 13a) and b) together with experimental data taken from Refs [16,17]. The data are fairly effectively reproduced. The allowed longitudinal multipoles are C0 and C2, whereas, the transverse multipoles are Ml and M3. The effects of these multipoles are evaluated using p-model space with HO potential. By combining the contributions of these multipolarities, we can deduce that there was no significant difference between the total longitudinal form factors in the low momentum transfer region as far as the single-particle potential is changed. Afterward, the SLy4 parameterization failed to reproduce the experimental data. The total transverse magnetic form factors are depicted in Fig. 13b). Inspection of these curves reveals that the p-model space predictions with SLy4 and WS potentials exhibit qualitative resemblance in shape and appear to be underestimated the experimental data. Whereas the prediction using HO is consistent with experimental data. Interestingly, the choice of the oscillator size parameter can give the best serves all form factors for displacing to high momentum transfer region.

4. Conclusions

Our study provides the theoretical framework for calculating the nuclear magnetic dipole and electric quadrupole moments taking into account the effects of the two-body effective interactions and the single-particle potentials. This method was implemented for Boron isotopes, furthermore, the electroexcitation form factors from low-lying states up to 6.129 MeV were also presented in which there were available experimental data. The present work leads to the following main conclusions. The Shell model calculations with p-model space with Skyrme type interaction give a good description for most of the selected isotopes. No significant difference was noticed for the μ and Q moments with experimental data, where, all signs for the experimental data are reproduced correctly. The electroexcitation form factors are substantially compatible with the general trends of the experimental data without any further parameter fitting. The two isovector form factors calculated in the present work, for the 1.740 and 5.164 MeV transitions, are characterized by the influent of the transverse M3 multipoles. In contrast, isoscalar transitions were observed mainly through their longitudinal form factors: All isoscalar transitions to natural-parity states have dominant C2 multipoles, whereas the Cl and C3 multipoles were most important. The longitudinal and transverse form factors for negative parity states are fairly well reproduced using the truncated NCSM model space.

1. G. Neyens, *Rep. Prog. Phys.* **66** (2003) 633.
2. I. Hamamoto, and B. R. Mottelson, *Scholarpedia* **7** (2012) 10693.
3. A. Kamal "*Nuclear Physics*" Springer-Verlag, Berlin, Heidelberg (2014).
4. R.A. Radhi, A. A. Alzubadi and A. H. Ali, *Phys. Rev. C* **97** (2018) 1.
5. P. J. Brussaard, and P. W. M. Glaudemans, *Shell Model Applications In Nuclear Spectroscopy* (Amsterdam: North Holand) (1977) and Lecture Notes in Nuclear Structure Physics B. Alex Brown, November 2005
6. A. A. Alzubadi, *Indian J. Phys.* **89** (2015) 619.
7. T. de Forest, J. D. Walecka, *Adv. Phys.* **15** (1966) 1.
8. B. A. Brown *et al*., *Phys. Rev. C* **32** (1985) 1127.
9. B. A. Brown and W. D. M. Rae, *Nucl. Data Sheets* **120** (2014) 115.
10. N. J. Stone, *At. Data Nucl. Data Tables* **90** (2005) 75.
11. M. Karl "Extensions to the No-Core Shell Model" Springer International Publishing Switzerland (2013).
12. National Nuclear Data Center (NNDC), http://www.nndc.bnl.gov/
13. T. Sumikama *et al*., *Phys. Rev. C* **74** (2006) 024327.
14. A. Cichocki, J. Dubach, R. S. Hicks and G. A. Peterson, *Phys. Rev. C* **51** (1995) 2406.
15. E.K. Warburton and B.A. Brown, *Phys. Rev. C* **46** (1992) 923.
16. M. C. Bouten and M. Bouten, *Nucl, Phys. A* **299** (1978) 141.
17. J. G. Booten and A.G. M. vanHees, *Nucl, Phys. A* **569** (1994) 510.